Chinese Journal of Aeronautics, (2016), xxx(xx): xxx–xxx

Chinese Society of Aeronautics and Astronautics
& Beihang University

Chinese Journal of Aeronautics

cja@buaa.edu.cn
www.sciencedirect.com

REVIEW ARTICLE

Variable stiffness design of redundantly actuated planar rotational parallel mechanisms

Li Kangkang, Jiang Hongzhou *, Cui Zuo, Huang Qun

School of Mechatronics Engineering, Harbin Institute of Technology, Harbin 150001, China

Received 6 March 2016; revised 25 March 2016; accepted 12 June 2016

KEYWORDS

Internal force;
Parallel mechanisms;
Redundantly actuated;
Robustness;
Variable stiffness

Abstract Redundantly actuated planar rotational parallel mechanisms (RAPRPMs) adapt to the requirements of robots under different working conditions by changing the antagonistic internal force to tune their stiffness. The geometrical parameters of the mechanism impact the performances of modulating stiffness. Analytical expressions relating stiffness and geometrical parameters of the mechanism were formulated to obtain the necessary conditions of variable stiffness. A novel method of variable stiffness design was presented to optimize the geometrical parameters of the mechanism. The stiffness variation with the internal force was maximized. The dynamic change of stiffness with the dynamic location of the mechanism was minimized, and the robustness of stiffness during the motion of the mechanism was ensured. This new approach to variable stiffness design can enable off-line planning of the internal force to avoid the difficulties of on-line control of the internal force.

1. Introduction

Planar parallel manipulators perform two translations along the x- and y-axes, and rotate through an angle around the z-axis, perpendicular to the plane. They have some potential advantages over serial robotic manipulators such as better accuracy, greater load capacity, and higher velocity and acceleration.[1,2] The redundantly actuated planar rotational parallel mechanism (RAPRPM) is a special type of planar parallel manipulator. It does not have the ability to move along the x- and y-axes, and only has a single degree of freedom, rotating around the z-axis. Meanwhile, the stiffness of rotation around the z-axis can be modulated by employing redundant actuation. The performances including inverse kinematics, forward kinematics, Jacobian matrix, workspace, singularity, and dexterity of planar parallel manipulators have been analyzed.[1–4] Stiffness modeling of a robotic manipulator is also one of the important issues that allows a user to evaluate its compatibility for certain tasks.[5] Based on biological studies of the muscular properties and the skeletal structures of fish, Cui and Jiang presented a robotic fish consisting of planar serial-parallel mechanisms, i.e., the RAPRPMs connecting to each other in series. It included rigid bodies, springs, dampers, and revolution joints. Their results showed that the swimming

* Corresponding author.
E-mail addresses: likangkang2006@126.com (K. Li), jianghz@hit.edu.cn (H. Jiang), cuizuo@yeah.net (Z. Cui), huangqunhq@126.com (Q. Huang).

Peer review under responsibility of Editorial Committee of CJA.

ELSEVIER Production and hosting by Elsevier

http://dx.doi.org/10.1016/j.cja.2016.07.001
1000-9361 © 2016 Chinese Society of Aeronautics and Astronautics. Production and hosting by Elsevier Ltd.

performance of the robotic fish was largely dependent on the body stiffness and the driven frequency.[6] Biological experiments of fish have shown that fish change their natural frequency by modulating the stiffness of their bodies to match the driving frequency. Then fish can employ resonance to improve their swimming efficiency.[7–9] Swimming fish that can tune their body stiffness by appropriately timed muscle contractions are able to maximize peak acceleration or swimming speed. The muscles are modeled as springs of constant stiffness.[10] To study the body stiffness of robotic fish consisting of planar serial-parallel mechanisms, it is important to study the stiffness design and stiffness control of the RAPRPM. Stiffness control schemes realized by employing redundant actuation can be broadly categorized as: passive stiffness control (PSC), feedback stiffness control (FSC), and active stiffness control (ASC).[11,12] PSC is a scheme that changes the stiffness of the mechanism by adding flexible elements to the original mechanism.[13,14] Because the stiffness of flexible elements cannot be changed much, the stiffness of the mechanism is changed less by using PSC. An FSC scheme chooses proportional coefficients in the positioning joint controllers that correspond to the desired characteristics for control of the end-effector.[15,16] However, the modulation of proportional coefficients of controllers may make the system unstable. An ASC scheme yields antagonistic forces in a redundantly actuated mechanism. The internal forces balance each other in a closed mechanism and do not perform any effective work, but generate end-effector stiffness.[17–20] An ASC scheme can significantly modulate the stiffness by modulating the internal force, which involves off-line planning of antagonistic actuator loads, so that one can obtain the desired object stiffness.[21–24] An ASC scheme is chosen to control the stiffness of the RAPRPM because of its advantages over other stiffness control schemes.

In addition, it is also meaningful to apply an ASC scheme to maintain constant stiffness and maximize the change of stiffness with the internal force. Sungcheul et al. introduced two indexes, one of which was suggested to make the minimum stiffness similar to the maximum stiffness at a given point and to ensure robustness and balance of the stiffness in all directions. The other index was used to maximize the stiffness in a fixed direction along the pathway.[25] Hence, for the RAPRPM whose stiffness changes with the dynamic location of a platform, applying an ASC scheme to enable on-line control of the internal force according to the dynamic location to keep the stiffness constant and to maximize the change of stiffness with the internal force, would increase the controlling difficulty and responding time. However, when applying an ASC scheme to enable off-line planning of the internal force to avoid the difficulties of on-line control, geometrical parameters are required to meet the following three requirements. Firstly, the amount of active stiffness variation with the internal force is maximum. Secondly, the proportion of active stiffness in total stiffness is maximum. Thirdly, the dynamic change of active stiffness with the rotating angle is minimum to ensure the robustness of stiffness during movement of the platform. In addition, optimization strategies such as particle swarm optimization and genetic algorithms have been widely used to minimize the power requirement for a planar parallel manipulator,[26] to compensate for compliance errors,[5] to obtain superior dexterous workspace,[27,28] or to maximize stiffness.[29,30] Similarly, the geometrical parameters are optimized to maximize the stiffness variation with the internal force and minimize the dynamic changes of total stiffness with the dynamic location of the mechanism.

2. Torsional stiffness of RAPRPM

2.1. Variable stiffness principle of RAPRPM

Cui and Jiang presented the structure of a compliant fish consisting of planar serial-parallel redundantly actuated mechanisms, as shown in Fig. 1,[6] in which the RAPRPMs connect each other in series. The capacity of the fish to modulate stiffness can be replicated by changing the stiffness of the RAPRPMs.[6] As one of a series, the working principle of a single RAPRPM is shown in Fig. 2. The top platform A_1OA_2 is supported by the middle rigid leg OB_3 and the elastic legs A_1B_1 and A_2B_2. $|l_1|$ is the length of the elastic leg A_1B_1. $|l_2|$ is the length of the elastic leg A_2B_2. The elastic legs A_1B_1 and A_2B_2 on both sides connect the rotating pairs of the upper revolute joints A_1 and A_2 on the top platform and the rotating pairs of the lower revolute joints B_1 and B_2 on the fixed platform $B_1B_2B_3$. r_a is the center distance of the upper revolute joints, while r_b is the center distance of the lower revolute joints. The middle rigid leg OB_3 is attached to the fixed platform. The top platform rotates around the rotating center O with a single degree-of-freedom. q is the rotating angle, the position where the rotating angle $q = 0$ rad is defined as the initial position, h is the distance between the rotating center O and the fixed platform, L_c is the distance between the rotating center O and the top platform, and $\boldsymbol{r}$ is the vector from the rotating center O to the upper revolute joints. The linear drivers C_1 and C_2 change the internal forces resulting from the elastic legs A_1B_1 and A_2B_2, respectively, and the internal forces balance each other to provide active stiffness in the closed mechanism. $\boldsymbol{f}$ is the outputting internal force of the leg. XOY is defined as the base coordinate fixed to the rotating center O, and its Y-axis parallels to OB_3. x_0Oy_0 is defined as the rotating coordinate fixed to the top platform.

The torsional stiffness K of the RAPRPM is defined as[25]

$$K = \frac{\partial Q}{\partial q} \tag{1}$$

where Q is the torque of the top platform.

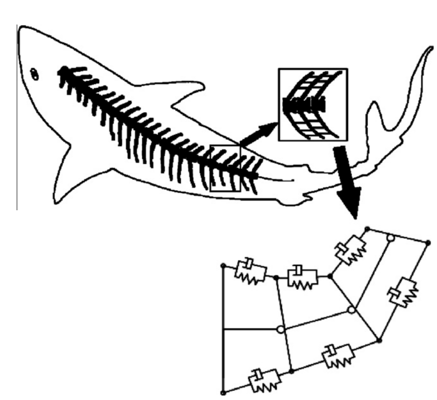

Fig. 1 Compliant fish with serial-parallel redundantly actuated mechanisms.

Please cite this article in press as: Li K et al. Variable stiffness design of redundantly actuated planar rotational parallel mechanisms, *Chin J Aeronaut* (2016), http://dx.doi.org/10.1016/j.cja.2016.07.001

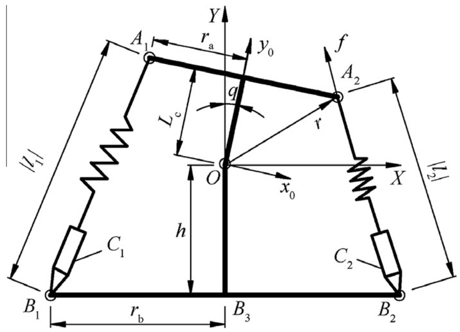

Fig. 2 Schematic of a single parallel mechanism.

As shown in Fig. 2, the torque Q of the top platform is defined as follows:

$$Q = \boldsymbol{r}^{\mathrm{T}}\boldsymbol{E}\boldsymbol{f} \tag{2}$$

where $\boldsymbol{r} = [x, y]^{\mathrm{T}}$. $\boldsymbol{E}$ is the two-dimensional rotational matrix, and $\boldsymbol{E} = \begin{bmatrix} 0 & 1 \\ -1 & 0 \end{bmatrix}$. The components of the internal force $\boldsymbol{f}$ are f_x and f_y, which can be written as

$$\boldsymbol{f} = [f_x, f_y]^{\mathrm{T}} = f_0 \boldsymbol{l}_{\mathrm{n}} \tag{3}$$

where f_0 is the amount of the internal force. $\boldsymbol{l}_{\mathrm{n}}$ is the unit vector of the elastic leg, and $\boldsymbol{l}_{\mathrm{n}} = \frac{\boldsymbol{l}}{|\boldsymbol{l}|}$, in which $\boldsymbol{l}$ is the vector of the elastic leg and $|\boldsymbol{l}|$ is the length of the elastic leg.

By substituting Eq. (2) into Eq. (1), the torsional stiffness is

$$K = \frac{\partial(\boldsymbol{r}^{\mathrm{T}}\boldsymbol{E}\boldsymbol{f})}{\partial q} = \frac{\partial \boldsymbol{r}^{\mathrm{T}}}{\partial q}\boldsymbol{E}\boldsymbol{f} + \boldsymbol{r}^{\mathrm{T}}\boldsymbol{E}\frac{\partial \boldsymbol{f}}{\partial q} \tag{4}$$

Stiffness consists of active stiffness and passive stiffness. By substituting Eq. (3) into Eq. (4), the torsional stiffness K can be expressed as:

$$K = f_0\left(\frac{\partial \boldsymbol{r}^{\mathrm{T}}}{\partial q}\boldsymbol{E}\boldsymbol{l}_{\mathrm{n}} + \boldsymbol{r}^{\mathrm{T}}\boldsymbol{E}\frac{\partial \boldsymbol{l}_{\mathrm{n}}}{\partial q}\right) + \boldsymbol{r}^{\mathrm{T}}\boldsymbol{E}\boldsymbol{l}_{\mathrm{n}}\frac{\partial f_0}{\partial q} \tag{5}$$

where the first item is the active stiffness K_{a} resulting from the internal force of the mechanisms and the second item is the passive stiffness K_{p} caused by the location. Hence, the active stiffness can be given by[25]

$$K_{\mathrm{a}} = f_0\left(\frac{\partial \boldsymbol{r}^{\mathrm{T}}}{\partial q}\boldsymbol{E}\boldsymbol{l}_{\mathrm{n}} + \boldsymbol{r}^{\mathrm{T}}\boldsymbol{E}\frac{\partial \boldsymbol{l}_{\mathrm{n}}}{\partial q}\right) \tag{6}$$

The passive stiffness is[31]

$$K_{\mathrm{p}} = \boldsymbol{r}^{\mathrm{T}}\boldsymbol{E}\boldsymbol{l}_{\mathrm{n}}\frac{\partial f_0}{\partial q} = \left(\frac{\partial f_0}{\partial \lambda}\frac{\partial \lambda}{\partial q}\right)\boldsymbol{r}^{\mathrm{T}}\boldsymbol{E}\boldsymbol{l}_{\mathrm{n}} \tag{7}$$

where λ is the stretch-shortening length of the elastic leg, $\frac{\partial \lambda}{\partial q} = \boldsymbol{r}^{\mathrm{T}}\boldsymbol{E}\boldsymbol{l}_{\mathrm{n}}$, $\frac{\partial f_0}{\partial \lambda} = k'$, and k' is the stiffness of the elastic leg. Therefore the passive stiffness K_{p} can be found from Eq. (7) as

$$K_{\mathrm{p}} = k'\left(\boldsymbol{r}^{\mathrm{T}}\boldsymbol{E}\boldsymbol{l}_{\mathrm{n}}\right)^2 \tag{8}$$

2.2. Active stiffness of RAPRPM

As shown in Fig. 2, the torque Q of the mechanisms consists of the torque Q_1 caused by the elastic leg A_1B_1 acting on the top platform and the torque Q_2 caused by the elastic leg A_2B_2 acting on the top platform. That is, $Q = Q_1 + Q_2$. Hence, the total torsional stiffness K of the mechanisms consists of the torsional stiffness K_1 resulting from the elastic leg A_1B_1 and the torsional stiffness K_2 resulting from the elastic leg A_2B_2. The total torsional stiffness K is expressed as

$$K = K_1 + K_2 \tag{9}$$

Hence, the active stiffness and passive stiffness resulting from elastic legs A_1B_1 and A_2B_2 must firstly be solved before solving the total torsional stiffness K of the mechanisms.

As shown in Fig. 2, $\boldsymbol{r}_1$ is the vector between the rotating center O and the point of action A_1 of the internal force $\boldsymbol{f}_1$, and $\boldsymbol{r}_1 = [x, y]^{\mathrm{T}}$, which can be described as

$$\boldsymbol{r}_1 = \boldsymbol{R}\overrightarrow{OA_1} \tag{10}$$

where $\boldsymbol{R}$ is the matrix for coordinate transformation from the rotating coordinate x_0Oy_0 to the fixed coordinate XOY. $\boldsymbol{R} = \begin{bmatrix} \cos q & -\sin q \\ \sin q & \cos q \end{bmatrix}$.[32,33] In coordinate x_0Oy_0, $\overrightarrow{OA_1} = \begin{bmatrix} -r_{\mathrm{a}} \\ L_{\mathrm{c}} \end{bmatrix}$.

The vector of the elastic leg A_1B_1 is

$$l_1 = \overrightarrow{B_3O} + \boldsymbol{r}_1 - \overrightarrow{B_3B_1} \tag{11}$$

where $\overrightarrow{B_3O} = \begin{bmatrix} 0 \\ l_0 - L_{\mathrm{c}} \end{bmatrix}$, $\overrightarrow{B_3B_1} = \begin{bmatrix} -r_{\mathrm{b}} \\ 0 \end{bmatrix}$, l_0 is the total height from the fixed platform to the top platform at the initial position, and $l_0 = L_{\mathrm{c}} + h$.

The vector $\boldsymbol{l}_1$ of the elastic leg A_1B_1 can be derived from Eq. (11) as below[31]:

$$\begin{aligned} \boldsymbol{l}_1 &= [x_1, y_1]^{\mathrm{T}} \\ &= [-r_{\mathrm{a}}\cos q - L_{\mathrm{c}}\sin q + r_{\mathrm{b}}, -r_{\mathrm{a}}\sin q + L_{\mathrm{c}}\cos q + l_0 - L_{\mathrm{c}}]^{\mathrm{T}} \end{aligned} \tag{12}$$

The vector between the rotating center O and the point of action A_2 of the internal force $\boldsymbol{f}_2$ is shown as follows:

$$\boldsymbol{r}_2 = \boldsymbol{R}\overrightarrow{OA_2} \tag{13}$$

where $\overrightarrow{OA_2} = \begin{bmatrix} r_{\mathrm{a}} \\ L_{\mathrm{c}} \end{bmatrix}$ in coordinate x_0Oy_0.

Similarly, the vector $\boldsymbol{l}_2$ of the elastic leg A_2B_2 is expressed as follows:

$$\begin{aligned} \boldsymbol{l}_2 &= [x_2, y_2]^{\mathrm{T}} \\ &= [r_{\mathrm{a}}\cos q - L_{\mathrm{c}}\sin q - r_{\mathrm{b}}, r_{\mathrm{a}}\sin q + L_{\mathrm{c}}\cos q + l_0 - L_{\mathrm{c}}]^{\mathrm{T}} \end{aligned} \tag{14}$$

The torque Q_1 resulting from the elastic leg A_1B_1 acting on the top platform and the torque Q_2 resulting from the elastic leg A_2B_2 acting on the top platform are in equilibrium, that is, $Q_1 + Q_2 = 0$. Therefore, the amount of internal force caused by the elastic leg A_2B_2 can be derived from Eq. (2) as follows:

$$f_{20} = \frac{-\boldsymbol{r}_1^{\mathrm{T}}\boldsymbol{E}\boldsymbol{l}_{1n}f_{10}}{\boldsymbol{r}_2^{\mathrm{T}}\boldsymbol{E}\boldsymbol{l}_{2n}} \tag{15}$$

where f_{10} is the amount of internal force caused by the elastic leg A_1B_1, $\boldsymbol{l}_{1n}$ is the unit vector of the elastic leg A_1B_1, and $\boldsymbol{l}_{2n}$ is the unit vector of the elastic leg A_2B_2.

The active stiffness resulting from the elastic leg A_1B_1 can be found by substituting Eqs. (10) and (12) into Eq. (6) as:

$$K_{1\mathrm{aq}} = \frac{\partial \boldsymbol{r}_1^{\mathrm{T}}}{\partial q} \boldsymbol{E} f_{10} \boldsymbol{l}_{1\mathrm{n}} + \boldsymbol{r}_1^{\mathrm{T}} \boldsymbol{E} f_{10} \frac{\partial \boldsymbol{l}_{1\mathrm{n}}}{\partial q} \tag{16}$$

The active stiffness resulting from the elastic leg A_1B_1 at the initial position is derived from Eq. (16) as

$$K_{1\mathrm{a}} = \frac{f_{10}}{|\boldsymbol{l}_{10}|^3} \left[-l_0^2 L_\mathrm{c}^2 + L_\mathrm{c} l_0 \left(l_0^2 + r_\mathrm{b}^2 - r_\mathrm{a}^2 \right) + l_0^2 r_\mathrm{a} (r_\mathrm{a} - r_\mathrm{b}) - r_\mathrm{a} r_\mathrm{b} (r_\mathrm{a} - r_\mathrm{b})^2 \right] \tag{17}$$

where $|\boldsymbol{l}_{10}|$ is the length of the elastic leg A_1B_1 at the initial position; consequently, from Eq. (12), $|\boldsymbol{l}_{10}| = \sqrt{(r_\mathrm{a} - r_\mathrm{b})^2 + l_0^2}$.

Similarly, the active stiffness resulting from the elastic leg A_2B_2 can be given as follows by substituting Eqs. (13) and (14) into Eq. (6):

$$K_{2\mathrm{aq}} = \frac{\partial \boldsymbol{r}_2^{\mathrm{T}}}{\partial q} \boldsymbol{E} f_{20} \boldsymbol{l}_{2\mathrm{n}} + \boldsymbol{r}_2^{\mathrm{T}} \boldsymbol{E} f_{20} \frac{\partial \boldsymbol{l}_{2\mathrm{n}}}{\partial q} \tag{18}$$

The stiffness k_1' of the elastic leg A_1B_1 is designed to be equal to the stiffness k_2' of the elastic leg A_2B_2, that is, $k_1' = k_2'$. Meanwhile, the length of the elastic leg A_1B_1 is equal to that of the elastic leg A_2B_2 at the initial position, that is, $|\boldsymbol{l}_{10}| = |\boldsymbol{l}_{20}|$. As is found from Eq. (15), the amount f_{10} of the internal force caused by the elastic leg A_1B_1 is equal to the amount f_{20} of the internal force caused by the elastic leg A_2B_2, that is, $f_{10} = f_{20}$. As is found from Eqs. (16) and (18), the active stiffness $K_{1\mathrm{a}}$ of the elastic leg A_1B_1 is equal to the active stiffness $K_{2\mathrm{a}}$ of the elastic leg A_2B_2, that is, $K_{1\mathrm{a}} = K_{2\mathrm{a}}$.

The total active stiffness K_a of the mechanisms at the initial position is the sum of the active stiffness $K_{1\mathrm{a}}$ and the active stiffness $K_{2\mathrm{a}}$. That is, $K_\mathrm{a} = 2K_{1\mathrm{a}}$. According to Eqs. (9) and (17), the total active stiffness is described as

$$K_\mathrm{a} = \frac{2f_{10}}{|\boldsymbol{l}_{10}|^3} \left[-l_0^2 L_\mathrm{c}^2 + L_\mathrm{c} l_0 \left(l_0^2 + r_\mathrm{b}^2 - r_\mathrm{a}^2 \right) + l_0^2 r_\mathrm{a} (r_\mathrm{a} - r_\mathrm{b}) - r_\mathrm{a} r_\mathrm{b} (r_\mathrm{a} - r_\mathrm{b})^2 \right] \tag{19}$$

As is found from Eq. (19), the active stiffness $K_\mathrm{a} = 0$ when $r_\mathrm{a} = r_\mathrm{b}$ with $L_\mathrm{c} = 0$ mm or $L_\mathrm{c} = l_0$, i.e., the internal force cannot tune the total torsional stiffness when the center distance of the upper revolute joints is equal to the center distance of the lower revolute joints when the rotating center is on the top platform or on the fixed platform. The condition of the internal force tuning the stiffness is to avoid the situation. In addition, Eq. (19) is a quadratic function of L_c, therefore, derived from Eq. (19), the amount of active stiffness K_a is maximum when L_c meets the following requirement:

$$L_\mathrm{c} = (r_\mathrm{b} - r_\mathrm{a})(r_\mathrm{b} + r_\mathrm{a})/(2l_0) + l_0/2 \tag{20}$$

Hence, L_c in Eq. (20) is the geometrical parameter that maximizes the amount of stiffness variation with the internal force.

ΔK_a is the difference between the maximum active stiffness K_{amax} and the minimum active stiffness K_{amin} during the rotation of the platform. K_{a0} is the active stiffness at the initial position. The ratio $\Delta K_\mathrm{a}/K_{\mathrm{a0}}$ is the maximum change of the active stiffness K_a during the rotation of the platform. Derived from Eqs. (16) and (18), as the center distance r_a of the upper revolute joints or the center distance r_b of the lower revolute joints increases, the maximum change of the active stiffness K_a during the rotation of the platform decreases.

The internal force of the elastic leg can be given as follows:

$$f_{10} = k_1' c |l_{10}| \tag{21}$$

where c is the ratio of the stretch-shortening length to the total length of the elastic leg.

The active stiffness is derived as follows by substituting Eq. (21) into Eq. (19):

$$K_\mathrm{a} = \frac{2k_1' c}{|\boldsymbol{l}_{10}|^2} \left[-l_0^2 L_\mathrm{c}^2 + L_\mathrm{c} l_0 \left(l_0^2 + r_\mathrm{b}^2 - r_\mathrm{a}^2 \right) + l_0^2 r_\mathrm{a} (r_\mathrm{a} - r_\mathrm{b}) - r_\mathrm{a} r_\mathrm{b} (r_\mathrm{a} - r_\mathrm{b})^2 \right] \tag{22}$$

2.3. Passive stiffness of RAPRPM

The passive stiffness resulting from the elastic leg A_1B_1 is derived by substituting Eqs. (10) and (12) into Eq. (8) as follows:

$$K_{1\mathrm{pq}} = k_1' \left(\boldsymbol{r}_1^T \boldsymbol{E} \boldsymbol{l}_{1\mathrm{n}} \right)^2 \tag{23}$$

The passive stiffness at the initial position is derived from Eq. (23) as follows:

$$K_{1\mathrm{p}} = \frac{k_1' [(l_0 - L_\mathrm{c}) r_\mathrm{a} + r_\mathrm{b} L_\mathrm{c}]^2}{|\boldsymbol{l}_{10}|^2} \tag{24}$$

Similarly, the passive stiffness resulting from the elastic leg A_2B_2 is derived as follows by substituting Eqs. (13) and (14) into Eq. (8):

$$K_{2\mathrm{pq}} = k_2' \left(\boldsymbol{r}_2^{\mathrm{T}} \boldsymbol{E} \boldsymbol{l}_{2\mathrm{n}} \right)^2 \tag{25}$$

It can be derived from Eqs. (23) and (25) that the passive stiffness $K_{1\mathrm{p}}$ resulting from the elastic leg A_1B_1 is equal to the passive stiffness $K_{2\mathrm{p}}$ resulting from the elastic leg A_2B_2 at the initial position. That is, $K_{1\mathrm{p}} = K_{2\mathrm{p}}$.

The total passive stiffness K_p of the mechanisms at the initial position is the sum of the two passive stiffness $K_{1\mathrm{p}}$ and $K_{2\mathrm{p}}$. That is, $K_\mathrm{p} = 2K_{1\mathrm{p}}$. According to Eqs. (9) and (24), the total passive stiffness is given as

$$K_\mathrm{p} = \frac{2k_1' [(l_0 - L_\mathrm{c}) r_\mathrm{a} + r_\mathrm{b} L_\mathrm{c}]^2}{|\boldsymbol{l}_{10}|^2} \tag{26}$$

2.4. Total stiffness of RAPRPM

The total stiffness K at the initial position is the sum of the total active stiffness K_a and the total passive stiffness K_p, which can be derived from Eqs. (5), (19), and Eq. (26) as:

$$K = \frac{2f_{10}}{|\boldsymbol{l}_{10}|^3} \left[-l_0^2 L_\mathrm{c}^2 + L_\mathrm{c} l_0 \left(l_0^2 + r_\mathrm{b}^2 - r_\mathrm{a}^2 \right) + l_0^2 r_\mathrm{a} (r_\mathrm{a} - r_\mathrm{b}) - r_\mathrm{a} r_\mathrm{b} (r_\mathrm{a} - r_\mathrm{b})^2 \right] + \frac{2k_1' [(l_0 - L_\mathrm{c}) r_\mathrm{a} + r_\mathrm{b} L_\mathrm{c}]^2}{|\boldsymbol{l}_{10}|^2} \tag{27}$$

In the case of Eq. (20), the amount of active stiffness variation with the internal force is maximum. The ratio of active to passive stiffness at the initial position is derived from Eqs. (22) and (26) as:

$$\frac{K_\mathrm{a}}{K_\mathrm{p}} = \frac{c \left(l_0^4 + r_\mathrm{a}^4 + 6r_\mathrm{a}^2 r_\mathrm{b}^2 + r_\mathrm{b}^4 + 2l_0^2 r_\mathrm{b}^2 + 2l_0^2 r_\mathrm{a}^2 - 4l_0^2 r_\mathrm{a} r_\mathrm{b} - 4r_\mathrm{a}^3 r_\mathrm{b} - 4r_\mathrm{a} r_\mathrm{b}^3 \right)}{\left[l_0 (r_\mathrm{a} + r_\mathrm{b}) + \frac{(r_\mathrm{b} + r_\mathrm{a})(r_\mathrm{a} - r_\mathrm{b})^2}{l_0} \right]^2} \tag{28}$$

It is derived from Eq. (28) that K_a/K_p increases as the center distance r_a of the upper revolute joints or the center distance r_b of the lower revolute joints decreases, i.e., as the center distance of the upper revolute joints or the center distance of the lower revolute joints declines, the proportion of the active stiffness in the total stiffness rises.

2.5. Stiffness optimization

A robotic fish can be constructed by RAPRPMs connecting each other in series. The capacity of the fish to modulate stiffness can be replicated by changing the stiffness of the RAPRPM,[6] so the stiffness of the robotic fish can be optimized by optimizing the stiffness and geometrical parameters of the RAPRPM. Under the conditions of ensuring the profile and the robustness of the body stiffness of the fish during a motion, by optimizing the geometrical parameters of the RAPRPM, the stiffness variation with the internal force was maximized to change its natural frequency to match the driving frequency in a large range.[7–9] In the stiffness optimization of the RAPRPM, the design variables were the center distances r_a and r_b. Because the profile and the cross section of the fish body determined the maximum center distances r_{amax} and r_{bmax}, the first constraining condition was that the center distance r_a was less than r_{amax}, and r_b was less than r_{bmax}. The second constraining condition was set as Eq. (20) to maximize the amount of active stiffness variation. The fish was required to swing from $q = 0$ to $q = 0.1$ rad during the swimming motion, so the third constraining condition was set so that $\Delta K_a/K_{a0}$ was less than the index μ to ensure the robustness of stiffness as the platform rotated from $q = 0$ to $q = 0.1$ rad. Maximizing K_a/K_p was set as the optimal objective to maximize the proportion of the active stiffness in the total stiffness. Therefore, by optimizing the geometrical parameters r_a and r_b, the stiffness variation of the fish body with the internal force was maximized. r_a and r_b can be obtained by solving the following optimization problem:

$$\text{Maximizing } \langle K_a/K_p \rangle \quad \text{Subject to} \begin{cases} r_a \leqslant r_{amax} \\ r_b \leqslant r_{bmax} \\ L_c = (r_b - r_a)(r_b + r_a)/(2l_0) + l_0/2 \\ \Delta K_a/K_{a0} \leqslant \mu \end{cases} \tag{29}$$

The constrained optimization problem of Eq. (29) was solved by using the function "fmincon" in MATLAB. For example, the stiffness of the elastic legs was $k'_1 = 4.1$ N/mm, the total height from the fixed platform to the top platform was $l_0 = 288$ mm, the maximum center distance $r_{amax} = 100$ mm, $r_{bmax} = 130$ mm, and the index $\mu = 0.1$. The results of optimization were $r_a = 22$ mm and $r_b = 130$ mm. While the index $\mu = 0.2$, the results of optimization were $r_a = 30$ mm and $r_b = 64$ mm.

3. Experimental verification

The schematic of the experimental setup of the RAPRPM is shown in Fig. 3. The top platform was supported by the middle rigid leg and the elastic legs on both sides. The elastic legs connected to the rotating pairs of the upper revolute joints and the lower revolute joints. The top platform rotated around the pin with a single degree-of-freedom, and the pin was also the rotating center of the top platform. The elastic legs on both sides consisted of the upper piston, the lower cylinder, and the middle spring. To modulate the active stiffness of the mechanism, the internal forces caused by the elastic legs could be modulated by moving the ring along the screw to change the length of spring stretch-shortening. The pin could be installed on different holes of the middle rigid leg to modulate the rotating center of the top platform. The bases on both ends of the elastic legs could be installed on different holes of the top platform and the fixed platform to modulate the center distances of the upper revolute joints and the lower revolute joints. The load torque was provided by the rotation of the top platform through applying a weight. The schematic of the signal collection system of the experimental setup is shown in Fig. 4, in which the rotating angle was converted from the measurements of the displacement sensors on both sides above the top platform. The internal forces of the elastic legs were measured by force sensors connected to the elastic legs on both sides. The experimental torsional stiffness was obtained by the ratio of the load torque to the measured rotating angle. In addition, a SimMechanics simulation model of an RAPRPM corresponding to the experimental setup is shown in Fig. 5, which consists of the top platform, elastic leg 1, elastic leg 2, and the middle rigid leg. The torque was applied to the top platform to produce a rotating angle. Torsional stiffness in the simulation was the ratio of the torque to the rotating angle. The theoretical calculation was also verified by the Matlab SimMechanics simulation.

When the center distance of the upper revolute joints was $r_a = 50$ mm and the center distance of the lower revolute joints was $r_b = 50$ mm, $r_a = r_b$. The stiffness of the elastic legs was $k'_1 = 4.1$ N/mm, and the total height from the fixed platform to the top platform was $l_0 = 288$ mm. The distance between the rotating center O and the top platform was $L_c = 0$ mm or $L_c = 288$ mm. By theoretical calculation, simulation, and experiment, the total stiffness K of $L_c = 0$ mm and $L_c = 288$ mm at the initial position changing with the internal force of the elastic leg f_{10} are shown in Fig. 6(a) and (b), respectively, and the result of simulation was very close to the theoretical result. In addition, the error between the experimental and the-

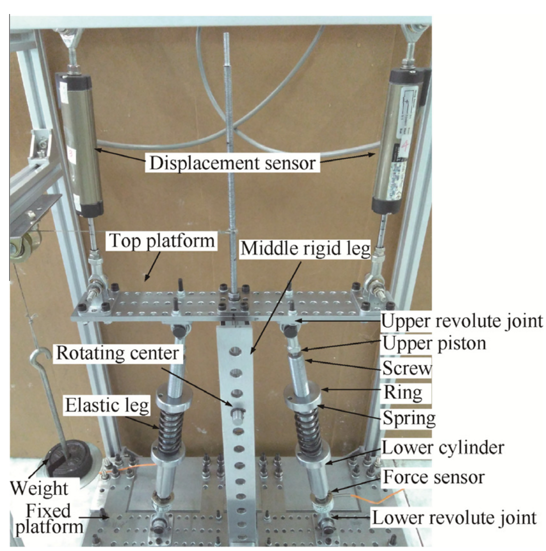

Fig. 3 Experimental setup of the RAPRPM.

Please cite this article in press as: Li K et al. Variable stiffness design of redundantly actuated planar rotational parallel mechanisms, *Chin J Aeronaut* (2016), http://dx.doi.org/10.1016/j.cja.2016.07.001

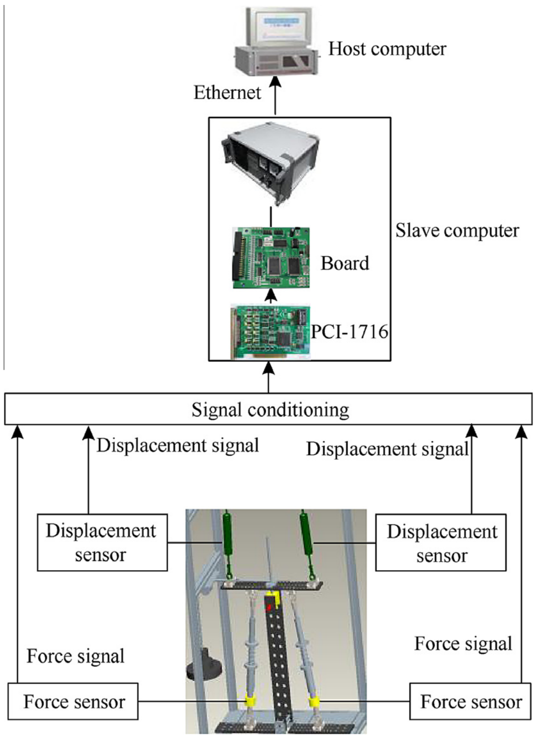

Fig. 4 Schematic of the signal collection system of the experimental setup.

oretical results was less than 10%, and because of the friction of the experimental setup, the total stiffness obtained by experiment was higher than that obtained by theory. It shows that the total stiffness changed little with the internal force, i.e., the internal force could not tune the total torsional stiffness when the center distance of the upper revolute joints was equal to the center distance of the lower revolute joints when the rotating center was on the top platform or on the fixed platform.

In the experiment, with reference to Eq. (5), the active stiffness K_a caused by a non-zero internal force was obtained by the total stiffness K when the internal force was non-zero, subtracting the total stiffness K when the internal force was zero which was also the passive stiffness K_p, i.e., $K_a = K - K_p$. The stiffness of the elastic legs was $k_1' = 4.1$ N/mm, the internal force was $f_{10} = 60$ N, and the total height from the fixed platform to the top platform was $l_0 = 288$ mm. The center distance of the upper revolute joints was $r_a = 50$ mm, and the center distance of the lower revolute joints was $r_b = 50$ mm. By theoretical calculation, simulation, and experiment, L_c is the distance between the rotating center and the top platform. The active stiffness K_a at the initial position changing with L_c is shown in Fig. 7. The curve tendencies of the active stiffness for theory, simulation, and experiment are similar to each other. It shows that in the case of Eq. (20), that is, $L_c = 144$ mm, the amount of active stiffness reaches the maximum.

K_a/K_p is the ratio of the active stiffness K_a to the passive stiffness K_p at the initial position. When the stiffness of the

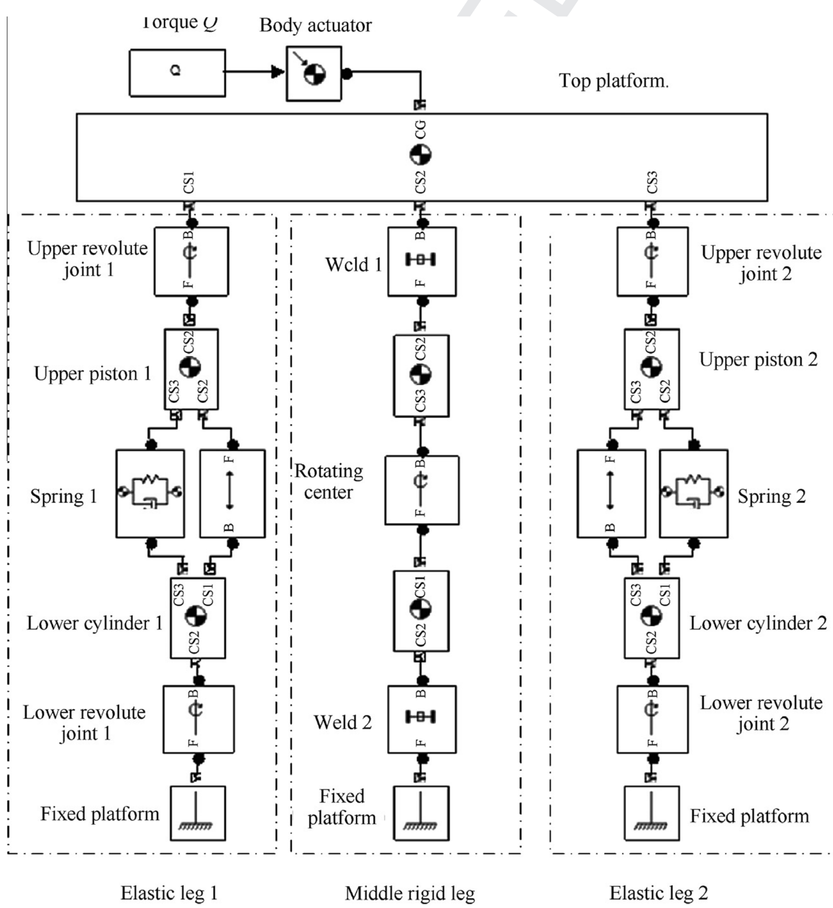

Fig. 5 SimMechanics simulation model.

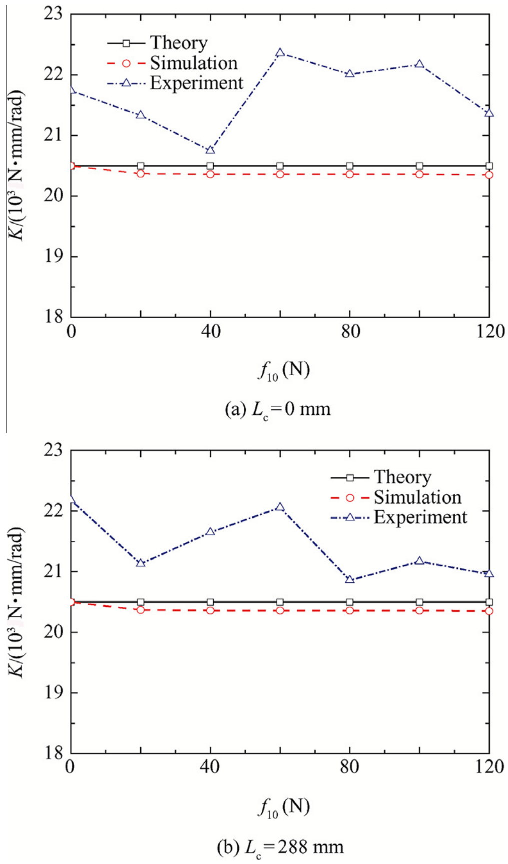

Fig. 6 Total stiffness variation with internal force.

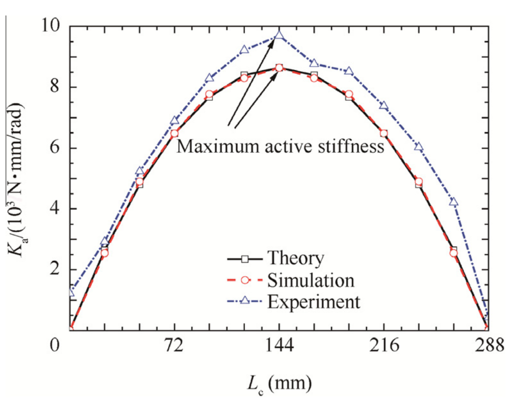

Fig. 7 Active stiffness variation with L_c.

elastic leg was $k_1' = 4.1$ N/mm, the internal force was $f_{10} = 60$ N, and L_c met the requirement of Eq. (20) to maximize the amount of active stiffness variation, by theoretical calculation, simulation, and experiment, K_a/K_p changed with different center distances r_a of the upper revolute joints and center distances r_b of the lower revolute joints, as shown in Fig. 8(a) and (b), respectively. The curve tendencies of K_a/K_p changing with respect to r_a or r_b by theory, simulation, and experiment are similar to each other. They show that K_a/K_p increased with the decrease of r_a or r_b, i.e., as the center distance of the upper revolute joints or the center distance of the lower revolute joints declined, the proportion of the active stiffness in the total stiffness rose.

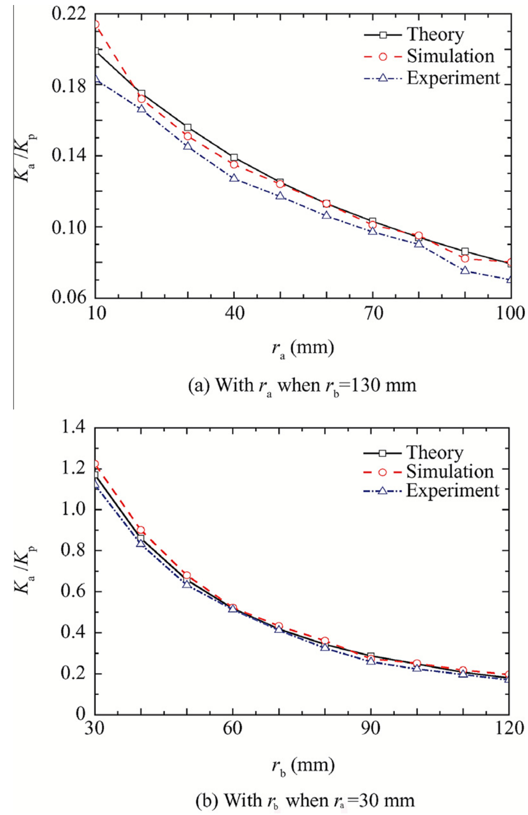

Fig. 8 K_a/K_p variation with r_a and r_b.

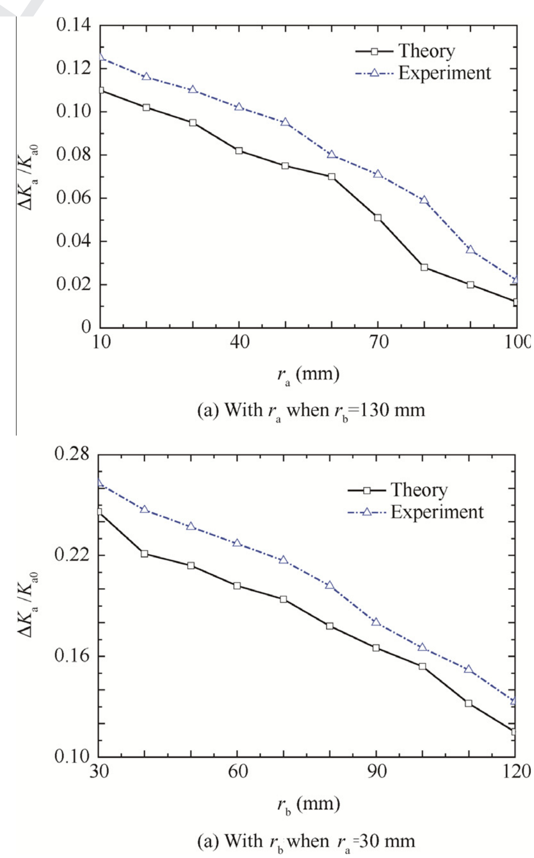

Fig. 9 $\Delta K_a/K_{a0}$ variation with r_a and r_b.

ΔK_a is the difference between the maximum active stiffness K_{amax} and the minimum active stiffness K_{amin} as the platform rotated from $q = 0$ to $q = 0.1$ rad. K_{a0} is the active stiffness at the initial position. The ratio $\Delta K_a/K_{a0}$ is the maximum change of the active stiffness K_a during the rotation of the platform. When the stiffness of the elastic legs was $k_1' = 4.1$ N/mm, the internal force was $f_{10} = 60$ N, and L_c met the requirement of Eq. (20) to maximize the amount of active stiffness variation, by theoretical calculation and experiment, for different center distances r_a of the upper revolute joints and center distances r_b of the lower revolute joints, the ratio $\Delta K_a/K_{a0}$ changing with r_a and r_b is shown in Fig. 9(a) and (b), respectively. The curve tendencies of $\Delta K_a/K_{a0}$ changing with r_a and r_b for the experiment are similar to the theoretical results. It shows that $\Delta K_a/K_{a0}$ decreased with the increase of r_a or r_b, i.e., as the center distance of the upper revolute joints or the center distance of the lower revolute joints increased, the maximum change of the active stiffness K_a during the rotation of the platform decreased.

4. Conclusions

(1) A novel design for stiffness variation was proposed to maximize the change of stiffness with the internal force and to minimize the dynamic change of stiffness with the dynamic location of the mechanism by optimizing the geometrical parameters of the mechanism. In addition, the relationships between the stiffness and the geometrical parameters were established.

(2) Internal force cannot tune the total torsional stiffness when the center distance of the upper revolute joints is equal to the center distance of the lower revolute joints, when the rotating center is on the top platform or on the fixed platform. The necessary condition of internal force tuning the stiffness is to avoid the situation.

(3) The positions of the rotating center maximizing the amount of stiffness variation with the internal force were obtained. The proportion of active stiffness in total stiffness rises as the center distance of the upper revolute joints or the center distance of the lower revolute joints declines. The maximum change of active stiffness during the rotation of the platform decreases as the center distance of the upper revolute joints or the center distance of the lower revolute joints increases. That is, the geometrical parameters maximize the change of stiffness with the internal force and minimize the dynamic change of total stiffness with the dynamic location of the mechanism.

Acknowledgement

This study was supported by the National Natural Science Foundation of China (No. 51275127).

Appendix A. Supplementary material

Supplementary data associated with this article can be found, in the online version, at http://dx.doi.org/10.1016/j.cja.2016.07.001.

References

1. Kucuk S. Simulation and design tool for performance analysis of planar parallel manipulators. *Simulat Trans Soc Model Simulat Int* 2012;**88**(5):542–56.
2. Merlet JP. Direct kinematics of planar parallel manipulators. In: *Proceedings of IEEE conference 1996 on robotics and automation; 1996 April 22–28; Minneapolis, Minnesota*; 1996. p. 3744–9.
3. Kucuk S. A dexterity comparison for 3-DOF planar parallel manipulators with two kinematic chains using genetic algorithms. *Mechatronics* 2009;**19**(6):868–77.
4. Merlet JP, Gosselin CM, Mouly N. Workspaces of planar parallel manipulators. *Mech Mach Theory* 1998;**33**(1):7–20.
5. Klimchik A, Chablat D, Pashkevich A. Stiffness modeling for perfect and non-perfect parallel manipulators under internal and external loadings. *Mech Mach Theory* 2014;**79**:1–28.
6. Cui Z, Jiang HZ. A study of the planar serial-parallel mechanism with various stiffness for a biotic compliant fish. In: *Proceedings of the ASME 2013 international mechanical engineering congress & exposition; 2013 November 13–21; San Diego, California, USA*; 2013. p. 1–6.
7. Epps BP, Alvarado PVY, Youcef-Toumi K, Techet AH. Swimming performance of a biomimetic compliant fish-like robot. *Exp Fluids* 2009;**47**(6):927–39.
8. Alvarado PV. Design of biomimetic compliant devices for locomotion in liquid environments. *J Dyn Syst Meas Contr* 2007;**128**:3–13.
9. Alvarado PV. *Design of biomimetic compliant devices for locomotion in liquid environments* [dissertation]. Massachusetts: Massachusetts Institute of Technology; 2007.
10. Tytell ED, Hsu CY, Williams TL, Cohen AH, Fauci LJ. Interactions between internal forces, body stiffness, and fluid environment in a neuromechanical model of lamprey swimming. In: *Proceedings of the 2010 national academy of sciences of the United States of America*; 2010. p. 19832–7.
11. Dasgupta BH, Mruthyunjaya TS. Force redundancy in parallel manipulators: theoretical and practical issues. *Mech Mach Theory* 1998;**33**(6):727–42.
12. Chakarov D. Study of the antagonistic stiffness of parallel manipulators with actuation redundancy. *Mech Mach Theory* 2004;**39**(6):583–601.
13. Mills JK. Hybrid actuator for robot manipulators: design, control and performance. *Mechatronics* 1993;**3**(1):19–38.
14. Mittal S, Tasch U, Wang Y. A redundant actuation scheme for independent modulations of stiffness and position of a robotic joint. *Mech Haptic Interf* 1993;**49**:247–56.
15. Yokoi K, Kaneko M, Tanie K. Direct compliance control of parallel link manipulators. In: *Proceedings of the 8th CISM—IFToMM symposium; Paris, France*; 1990. p. 224–51.
16. Yokoi K, Kaneko M, Tanie K. Direct compliance control for a parallel link arm. *Trans Jpn Soc Mech Eng* 1989;**55**(515):1690–6.
17. Gardner JF, Kumar V, Ho JH. Kinematics and control of redundantly actuated closed chains. In: *Proceedings of the 1989 IEEE international conference on robotics and automation; Scottsdale*; 1989. p. 418–24.
18. Nahon MA, Angeles J. Force optimization in redundantly actuated closed kinematic chains. In: *Proceedings of the 1989 IEEE international conference on robotics and automation; Scottsdale*; 1989. p. 951–6.
19. Tadokoro S. Control of parallel mechanisms. *Adv Robot* 1993;**8**(6):559–71.
20. Cho W, Tesar D, Freeman RA. The dynamic and stiffness modeling of general robotic manipulator systems with antagonistic actuation. In: *Proceedings of the 1989 IEEE international conference on robotics and automation*; 1989. p. 1380–7.
21. Yi BJ, Freeman RA. Geometric characteristics of antagonistic stiffness in redundantly actuated mechanisms. In: *Proceedings of*

the 1989 IEEE international conference on robotics and automation; 1993. p. 654–61.

22. Yi BJ, Oh SR. Analysis of a 5-bar finger mechanism having redundant actuators with applications to stiffness. In: *Proceedings of the 1989 IEEE international conference on robotics and automation; Albuquerque*; 1997. p. 759–65.
23. Yi BJ, Freeman RA, Tesar D. Open-loop stiffness control of overconstrained mechanisms/robotic linkage systems. In: *Proceedings of the 1989 IEEE international conference on robotics and automation*; 1989. p. 1340–5.
24. Adli M, Ito K, Hanafusa H. A method for modulating the contact compliance in objects held by dual-arm robots. In: *Proceedings of the 1995 IEEE international conference on recent advances in mechatronics; Istanbul, Turkey*; 1995. p. 1065–72.
25. Sungcheul L, Sitae K, Woosung I, Moonki K, Jay IJ, Jongwon K. Experimental verification of antagonistic stiffness planning for a planar parallel mechanism with 2-DOF force redundancy. *Robotica* 2011;**29**(7):547–54.
26. Kucuk S. Energy minimization for 3-RRR fully planar parallel manipulator using particle swarm optimization. *Mech Mach Theory* 2013;**62**(4):129–49.
27. Toz M, Kucuk S. Dimensional optimization of 6-DOF 3-CCC type asymmetric parallel manipulator. *Adv Robot* 2014;**28**(9):625–37.
28. Marc A, Roger B. The synthesis of three-degree-of-freedom planar mechanisms with revolute joints (3-RRR) for an optimal singularity-free workspace. *J Robot Syst* 2004;**21**(5):259–74.
29. Chi Z, Zhang D, Xia L, Zhen G. Multi-objective optimization of stiffness and workspace for a parallel kinematic machine. *Int J Mech Mater Des* 2012;**9**(3):281–93.
30. Arsenault M, Boudreau R, Arsenault M. Synthesis of planar parallel mechanisms while considering workspace, dexterity, stiffness and singularity avoidance. *J Mech Des* 2006;**128**(12):69–78.
31. Shin H, Lee S, Jeong JI, Jongwon K. Antagonistic stiffness optimization of redundantly actuated parallel manipulators in a predefined workspace. In: *Proceedings of the 1995 IEEE/ASME international conference on transactions on mechatronics*; 2013. p. 1161–9.
32. Dai XL, Huang QT, Jiang HZ, Han JW. Kinematics analysis of a 3-dof rotational parallel mechanism. In: *2008 international workshop on modelling, simulation and optimization*; 2008. p. 404–7.
33. Tian TZ, Jiang HZ, Tong ZZ, He JF, Huang QT. An inertial parameter identification method of eliminating system damping effect for a six-degree-of-freedom parallel manipulator. *Chin J Aeronaut* 2015;**12**(2):582–92.

Li Kangkang is a Ph. D. candidate in the School of Mechatronics Engineering at Harbin Institute of Technology. His area of research includes variable stiffness design of serial-parallel redundantly actuated mechanisms and robotic fish.

Jiang Hongzhou received his B.S. degree from Dalian Jiaotong University in 1993 and his M.S. and Ph.D. degrees from Harbin Institute of Technology, China in 1996 and 2000, respectively. He is currently a professor in the School of Mechatronic Engineering at Harbin Institute of Technology. His research interests include parallel manipulators, biomimetic robotics, system simulation, and control system development.

Cui Zuo is a Ph. D. candidate in the School of Mechatronics Engineering at Harbin Institute of Technology. His area of research includes biomimetic robotics.

Huang Qun is a M.S. student in the School of Mechatronics Engineering at Harbin Institute of Technology, where he received his B.S. degree in 2015. His area of research includes dynamics of serial-parallel redundantly actuated mechanisms.